# π-Bridge-Independent 2-(Benzo[c][1,2,5]thiadiazol-4-ylmethylene)malononitrile-Substituted Nonfullerene Acceptors for Efficient Solar Cells

Article

# #-Bridge-Independent 2-(Benzo[c][1,2,5]thiadiazol-4-ylmethylene)malononitrile-Substituted Nonfullerene Acceptors for Efficient Solar Cells

Kai Wang, Yuliar Firdaus, Maxime Babics, Federico Cruciani, Qasim Saleem, Abdulrahman El Labban, Maha A. Alamoudi, Tomasz Marszalek, Wojciech Pisula, Frédéric Laquai, and Pierre M. Beaujuge

*Chem. Mater.*, **Just Accepted Manuscript** • DOI: 10.1021/acs.chemmater.6b00131 • Publication Date (Web): 25 Feb 2016

# π-Bridge-Independent 2-(Benzo[*c*][1,2,5]thiadiazol-4-ylmethylene)malononitrile-Substituted Nonfullerene Acceptors for Efficient Solar Cells

Kai Wang,[†,§] Yuliar Firdaus,[†,§] Maxime Babics,[†] Federico Cruciani,[†] Qasim Saleem,[†] Abdulrahman EI Labban,[†] Maha A. Alamoudi,[†] Tomasz Marszalek,[‡] Wojciech Pisula,[‡,#] Frederic Laquai,[†] and Pierre M. Beaujuge[†,*]

[†]*Physical Sciences and Engineering Division, Solar & Photovoltaic Engineering Research Center (SPERC), King Abdullah University of Science and Technology (KAUST), Thuwal 23955-6900, Saudi Arabia*

[‡]*Max Planck Institute for Polymer Research, Anckermannweg 10, D-55128 Mainz, Germany*

[#]*Department of Molecular Physics, Faculty of Chemistry, Lodz University of Technology, Zeromskiego 116, 90-924 Lodz, Poland*

*Supporting Information Placeholder*

**ABSTRACT:** Molecular acceptors are promising alternatives to fullerenes (*e.g.* $PC_{61}/_{71}BM$) in the fabrication of high-efficiency bulk-heterojunction (BHJ) solar cells. While solution-processed polymer-fullerene BHJ devices have recently met the 10% efficiency threshold, molecular acceptors have yet to prove comparably efficient with polymer donors. At this point in time, it is important to forge a better understanding of the design parameters that directly impact small-molecule (SM) acceptor performance in BHJ solar cells. In this report, we show that 2-(benzo[*c*][1,2,5]thiadiazol-4-ylmethylene)malononitrile (BM)-terminated SM acceptors can achieve efficiencies as high as 5.3% in BHJ solar cells with the polymer donor PCE10. Through systematic device optimization and characterization studies, we find that the nonfullerene analogues (**FBM**, **CBM** and **CDTBM**) all perform comparably well, independent of the molecular structure and electronics of the π-bridge that links the two electron-deficient BM end groups. With estimated electron affinities within range of those of common fullerenes (4.0-4.3 eV), and a wider range of ionization potentials (6.2-5.6 eV), the SM acceptors absorb in the visible spectrum and effectively contribute to the BHJ device photocurrent. BM-substituted SM acceptors are promising alternatives to fullerenes in solution-processed BHJ solar cells.

## Introduction

Fullerene acceptors, such as phenyl-$C_{61}$-butyric acid methyl ester or its $C_{71}$ analogue ($PC_{61}BM$, $PC_{71}BM$), have long represented the most effective electron-transport material in solution-processed bulk-heterojunction (BHJ) solar cells with π-conjugated polymer and small-molecule (SM) donors.[1-5] Fullerenes have large electron affinity (EA) and ionization potential (IP) values of *ca.* 4.1-4.3 eV and 5.9 eV, respectively, favorable electron mobilities on the order of $10^{-3}$ $cm^2(Vs)^{-1}$ in diode configurations, and isotropic carrier transport characteristics. In addition, they tend to develop intimately mixed percolation networks with polymer and SM donors, with domain sizes on the order of exciton diffusion lengths common to *organic electronics* (5-20 nm). Achieving comparable characteristics with alternative, planar π-conjugated molecular systems has shown to be a remarkably challenging exercise over the years,[6-10] and fullerenes remain the best-performing electron acceptors to date, yielding power conversion efficiencies (PCEs) of over 10% in BHJ solar cells with various polymer and SM donors.[11-14] It is worth noting that planar SM acceptors can combine tunable EA and IP values, visible spectral absorption and charge transport characteristics by design.[15] In principle, these fullerene alternatives should rival PCBM acceptors, whose absorption is mostly confined to the short-wavelength range of the UV-visible spectrum (*ca.* 300-500 nm). Despite compelling potential benefits over PCBM acceptors, including synthetic accessibility and modularity, the reasons why planar SM acceptors are not currently outperforming their fullerene counterparts remain a matter of some debate.[16-19] In turn, at this point in time, it is important to forge a better understanding of the design parameters that directly impact nonfullerene acceptor performance in BHJ solar cells.

Given the outstanding headway made in the past recent years in optimizing polymer and SM donor performance using fullerenes as model systems,[5,20-22] a case could be made that further BHJ solar cell efficiency improvements

should come from the optimization of the acceptor component. Several approaches are currently being explored in the design of nonfullerene acceptors,[17-18] generally using some of the following motifs to promote the electron-transport properties of polymer[9,23-25] and/or SM[17,26] systems: perylene diimide (PDI),[7,16,27-33] naphthalene diimides (NDI),[34-36] diketopyrrolopyrrole (DPP),[24,37-39] benzothiadiazole and analogues, and more recently rhodanines.[43-45] In the design of efficient SM acceptors, the use of motifs that can induce "out-of-plane" molecular geometries and limit excess SM crystallization in BHJ thin films has been described as an important parameter in several studies.[45-47] However, it is worth noting that (i) published polymer and SM acceptor systems do not currently outperform PCBM acceptors,[17-18,25,48-49] and (ii) more planar and comparably efficient systems are concurrently being reported.[38,44,50-51] Taking high carrier mobilities as an important consideration in the design of nonfullerene acceptors, the more planar systems should ultimately prove more efficient.[29] At present, several SM systems can achieve PCEs >6% in BHJ solar cells with specific polymer donors,[27,50,52-54] but most reported systems have met with PCE limits of 5% or less, and it remains critically important to continue examining the key design principles that will help identify SM acceptors outperforming their fullerene counterparts. For practical reasons, the most synthetically accessible systems will likely become the most relevant.

Another promising electron-accepting motif for the design of SM acceptors may be 2-(benzo[c][1,2,5]thiadiazol-4-ylmethylene)malononitrile (BM). Used in earlier work on SM donors for vacuum-deposited SM solar cells,[55] BM end groups induce high EAs (*i.e.* low-lying LUMOs), efficient intramolecular charge transfer characteristics with electron-rich motifs, and promote rigid-planar structures that favors the development of specific intermolecular interactions (*e.g.* π–π stacking) which, in turn, tend to improve carrier mobilities.[56-58] While BM-substituted SM donors have led to high-efficiency (vacuum-deposited) triple-junction solar cells of PCEs >11%,[59] this motif has rarely been used in the design of nonfullerene acceptors.[57] Recent work has, however, shown that BM-substituted SM acceptors can yield PCEs >4% in BHJ solar cells with the polymer donor PBDTTT-C-T.[60] In this contribution, we report on a set of three solution-processable SM acceptors composed of BM end groups linked via distinct π-bridges: fluorene (**FBM**), carbazole (**CBM**) and cyclopenta[2,1-*b*:3,4-*b*']dithiophene (**CDTBM**) (Chart 1). The π-bridges are shown to fine-tune the electronics and the molecular conformation of the SM acceptors, imparting estimated EAs within range of those of common fullerene acceptors (4.0-4.3 eV) and a wider range of IPs (6.2-5.6 eV). The nonfullerene analogues absorb in the visible spectrum (**FBM**, **CBM**: 400-600 nm; **CDTBM**: 500-850 nm), and we show that BHJ solar cells efficiencies >5% can be achieved with the polymer donor PCE10 (Chart 1). Importantly, we demonstrate that the SM analogues all perform comparably well in BHJ solar cells, independent of the molecular structure and electronics of the π-bridge that links the two electron-deficient BM end groups, suggesting that BM-substituted SMs are a very promising class of nonfullerene acceptors.

Chart 1. 2-(Benzo[*c*][1,2,5]thiadiazol-4-ylmethylene)-malononitrile-substituted SM Acceptors: FBM, CBM and CDTBM.

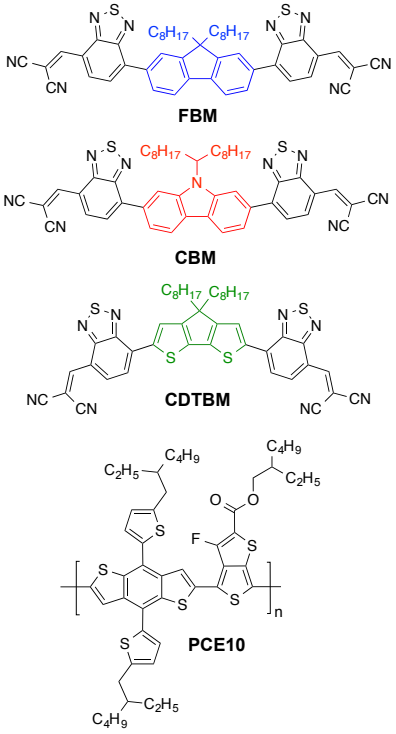


## Results and Discussion

### Design, Synthesis and Material Properties

The design of molecular acceptors with finite, relatively short conjugation lengths, as alternatives to fullerenes, has practical implications that span synthetic accessibility and potentially low synthetic costs compared to those associated with the synthesis of PCBM analogues (subject to extensive purification protocols). The ability to tune the optoelectronic properties (*i.e.* EAs, IPs, spectral absorption, etc.) of SM acceptors by design is another clear benefit given that fullerene derivatizations have either modest effects on their optoelectronics[1,3-4] or tend to lead to lower material performance in BHJ solar cells with polymer donors.[21] A few recently published studies[17,57] point to the relevance of small-size, "linear", solution-processable molecular acceptors as PCBM replacements, some with promising BHJ solar cell efficiencies >2%.[18,43,49] Following these considerations, the synthetic route to **FBM** and **CBM** involve the two key steps depicted in Scheme 1: (i) Pd-mediated Suzuki cross-coupling between the diboronic acid bis(pinacol) esters of fluorene or carbazole and 7-bromobenzo[*c*][1,2,5]thiadiazole-4-carbaldehyde, and (ii) Knoevenagel condensation of intermediates **1** and **2** with malononitrile; see details in the Supporting Information, SI. The synthetic route to **CDTBM** (Scheme 1) involves a microwave-assisted direct Pd-mediated Stille cross-coupling between 4,4-dioctyl-2,6-bis(trimethylstannyl)-4*H*-cyclopenta[2,1-*b*:3,4-*b*']dithiophene and 2-((7-bromobenzo[*c*][1,2,5]thiadiazol-4-yl)methylene)malononitrile. After sequential purifications

**Scheme 1. Syntheses SM Acceptors: FBM, CBM and CDTBM.**

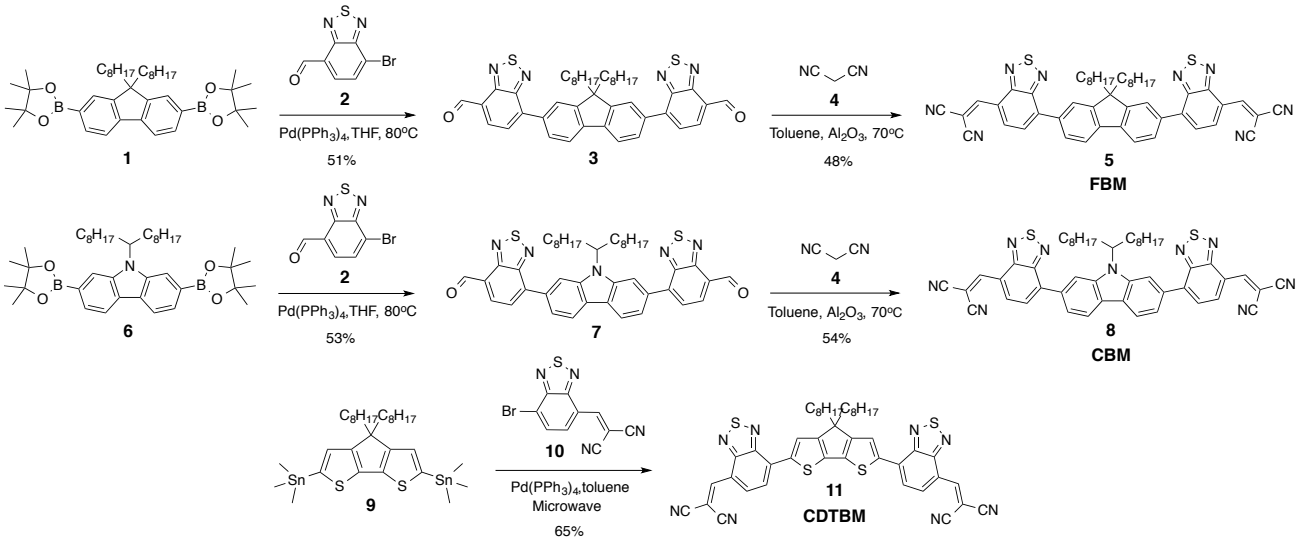


via column chromatography and recycling SEC (see details in SI), the SM acceptors **FBM** and **CBM** were collected as dark red solids in overall 45-55% yields, and **CDTBM** was obtained as a dark blue-green solid in a yield of *ca.* 65%. All three SM systems were found to be soluble in common organic solvents such as dichloromethane, chloroform, 1-chlorobenzene and 1,2-dichlorobenzene (appropriate solvents in the making of BHJ solar cells with established polymer donors, such as PCE10). Further synthetic details and structural analyses including $^{1}$H NMR, $^{13}$C NMR, and high-resolution mass spectrometry (HRMS) for all intermediates and products are provided in the SI.

First-level density functional theory (DFT) calculations (Fig. S2) show that the BM end groups tend to localize electron density on the periphery of the LUMOs in **FBM** and **CBM** SM acceptors, while the π-electron system is more delocalized and quinoidal in character in **CDTBM**; DFT at the B3LYP/6-31G(d,p) level with Gaussian 09 (Revision C.01) (cf. details in SI). These effects correlate with the "out-of-plane" geometry of **FBM** and **CBM** (Fig. S1), for which dihedral angles of *ca.* 34° and 32°, respectively, exist between the fluorene/carbazole motifs and the BM end groups; results consistent with prior calculations. In contrast, the SM acceptor **CDTBM** is expected to be relatively planar and its π-system more delocalized in the ground state (see HOMO of **CDTBM** in Fig. S2). Although side chains play an important role in molecular self-assembly, it is commonly assumed that the electronic properties and backbone geometry of single isolated π-conjugated systems are well represented in gas phase calculations where side chains are swapped for methyl groups (to optimize computational time).

Figure 1 shows the thin-film UV-Vis optical absorption spectra of **FBM**, **CBM** and **CDTBM** in terms of absorption coefficients (in the range 2.6-2.9 x $10^4$ $cm^{-1}$ at the longer-wavelength peak maxima). While **FBM** and **CBM** are found to have comparable onsets of absorption (*ca.* 590 and 610 nm, respectively) and, in turn, equivalent optical bandgap ($E_{opt}$) values of *ca.* 2 eV, **CDTBM** shows a significantly more red-shifted onset of absorption (*ca.* 850 nm) and a narrower $E_{opt}$ of *ca.* 1.5 eV. These differences can, in part, be explained by the larger extent of planarity expected in **CDTBM** compared to the "out-of-plane" conformations seen in **FBM** and **CBM** (Fig. S1). The solution and thin-film UV-Vis absorption spectra of the three SM acceptors **FBM**, **CBM** and **CDTBM** are overlaid in Figure S3. A comparison of the spectral absorption in solution and in the neat films shows that **CDTBM** undergoes a substantially more pronounced red-shift of *ca.* 100 nm (compared to *ca.* 40 nm for **FBM** and **CBM**; referenced to the onset), suggesting a relatively strong propensity to form ordered aggregates in thin films. In solution, however, the absence of long-wavelength absorption shoulders in the spectra of all SM acceptors indicate that the molecules are not prone to π-aggregate formation and can be well dispersed.

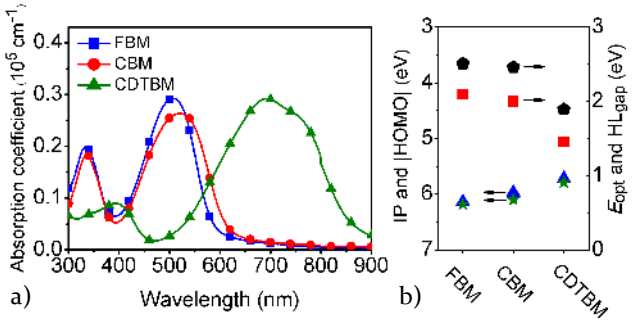


**Figure 1. (a)** Superimposed thin-film UV-Vis optical absorption spectra of **FBM**, **CBM** and **CDTBM** (absorption coefficients are represented). **(b)** PESA-estimated ionization potentials (IP, triangles), optical bandgaps ($E_{opt}$, squares) estimated from the onset of the UV-Vis absorption spectra (films), DFT-calculated HOMO energy levels (|HOMO|, absolute value, stars) and HOMO→LUMO gaps ($HL_{gap}$, pentagons) for the SMs; obtained at the B3LYP/6-31G(d,p) level.

The ionization potentials (IPs) of the SM acceptors were determined via photoelectron spectroscopy in air (PESA) (cf. details in SI): *ca.* 6.1 eV for **FBM**, *ca.* 6.0 eV for

**CBM**, and *ca.* 5.7 eV for **CDTBM**; expectedly large IP values within range of those commonly inferred for fullerene acceptors, and only slightly larger than the HOMO energy levels of *ca.* 6.2 eV, 6.1 eV and 5.8 eV (respectively) inferred from our DFT calculations. Table 1 provides further details, including electrochemically-estimated IPs and EAs (cf. details in SI), and bangdap estimations obtained from the DFT calculations ($HL_{gap}$). Figure S5 shows the reduction scans from which the electrochemically-estimated EAs were inferred: *ca.* 4.1 eV for **FBM**, *ca.* 4.1 eV for **CBM**, and *ca.* 4.3 eV for **CDTBM**; values within range of those of common fullerene acceptors such as $PC_{61}BM$ and $PC_{71}BM$ (4.1-4.3 eV).

The thermogravimetric analyses (TGA) given in Figure S6 show that the SM acceptors **FBM**, **CBM** and **CDTBM** are thermally stable in nitrogen atmosphere until *ca.* 350°C (*ca.* 5% weight loss observed at 373°C; 361°C and 432 °C, respectively). The differential scanning calorimetry (DSC) analyses shown in Figure S7 for **FBM** and **CBM** do not show any specific characteristic phase transitions, but the DSC traces of **CDTBM** indicate that a phase transition occurs in the range 80-100 °C, tentatively assigned to a melt in light of the apparent first order solidification peak on the reverse (cooling) scan (cf. details in SI).

The grazing incidence wide-angle X-ray scattering plots (GIWAXS; cf. details in SI) for neat films of **FBM**, **CBM** and **CDTBM** in Figure S8 indicate that the SM acceptors form relatively disordered films, without long-range ordering characteristics. In particular, the absence of scattering reflections in the 2D patterns of **FBM** and **CBM** (Fig. S8a and S8b) supports the idea that amorphous morphologies prevail in thin films made with these two SM analogues. Meanwhile, the scattering peak intensity seen in the 2D pattern of **CDTBM** along $q_z$ (0.2-0.5 $Å^{-1}$) and the weak π-stacking reflection centered along $q_{xy}$ (ca. 1.75 $Å^{-1}$) suggest the presence of edge-on-oriented aggregates in thin films (Fig. S8c). We note, however, that the absence of any pronounced scattering intensity at high $q$ values (1.5-2 $Å^{-1}$) in neat films of **FBM**, **CBM** and **CDTBM** implies that the SM aggregates are not correlated along the π-stacking direction.

**Table 1. Summary of Optoelectronic Parameters for the SM Acceptors: FBM, CBM and CDTBM.**

| SM Acceptor | $\lambda_{abs}$/sol (nm) (log ε) | $\lambda_{abs}$/film (nm) (log ε) | IP[a] (eV) | EA[b] (eV) | $E_{opt}$[c] (eV) | IP[d] (eV) | EA[d] (eV) | $E_{echem}$[d] (eV) | \|HOMO\|[e] (eV) | \|LUMO\|[e] (eV) | $HL_{gap}$[e] (eV) |
|---|---|---|---|---|---|---|---|---|---|---|---|
| **FBM** | 486 (5.18) | 501 (4.46) | 6.14 | 4.03 | 2.11 | 6.25 | 4.14 | 2.11 | 6.18 | 3.67 | 2.51 |
| **CBM** | 497 (5.20) | 517 (4.43) | 5.97 | 4.04 | 2.02 | 6.05 | 4.13 | 1.92 | 6.10 | 3.64 | 2.46 |
| **CDTBM** | 681 (5.34) | 701 (4.47) | 5.72 | 4.27 | 1.45 | 5.69 | 4.28 | 1.41 | 5.79 | 3.90 | 1.89 |

[a]Estimated by photoelectron spectroscopy (PESA). [b]Inferred from PESA-estimated IPs and $E_{opt}$ values. [c]Optical bandgaps estimated from the onset of the UV-Vis absorption spectra (films). [d]Estimated from cyclic voltammetry (CV) measurements; IP=$E_{onset,ox}$+5.1 eV and EA=$E_{onset,red}$+5.1 eV (absolute values), $E_{echem}$=IP-EA. [e]DFT-calculated HOMO and LUMO energy levels (absolute values), and HOMO→LUMO gaps ($HL_{gap}$); obtained at the B3LYP/6-31G(d,p) level.

## Device Testing and Characterizations

Thin-film BHJ solar cells with the inverted device structure ITO/*a*-ZnO[61]/PCE10:SM/$MoO_3$/Ag (device area: 0.1 $cm^2$) were fabricated and tested under AM1.5G solar illumination (100 mW/$cm^2$). The cells with optimized PCE10:SM blend ratios (PCE10:**FBM**, 4:6 wt/wt; PCE10:**CDTBM**, 4:6 wt/wt; PCE10:**CBM**, 3:7 wt/wt) were cast from chlorobenzene (CB) (cf. details in SI, active layer thicknesses: Avg. 65 nm); the control PCE10:$PC_{71}BM$ (4:6 wt/wt) devices were cast from chlorobenzene (CB) according to established optimized protocols (cf. details in SI).[62] Figure 2a depicts the current-voltage (*J-V*) characteristics of optimized **FBM**, **CBM** and **CDTBM**-based BHJ solar cells with the polymer donor PCE10. As shown in Table 2 (device statistics provided in the SI, Tables S1 and S2), "as-cast" BHJ devices made from the SM acceptors **FBM**, **CBM** and **CDTBM** all achieved substantial average PCE values of *ca.* 4% (Max. 4.6% obtained for **CDTBM**), with high short-circuit currents ($J_{SC}$) >9 mA/$cm^2$, but relatively modest fill-factor (*FF*) values in the range 44-53%. Optimized BHJ devices made from blends containing 0.8-2% (v/v) of the processing additive 1-chloronaphthalene (CN) or 1,8-diiodooctane (DIO) showed improved $J_{SC}$ (10-12 mA/$cm^2$) and *FF* (50-60%) values, and reached higher PCEs of *ca.* 5% (Max. 5.3% obtained with **CBM**). Small-molecule additives, such as CN and DIO, are now commonly used in the optimization of BHJ solar cells,[63-64] inducing changes in the blend morphologies and/or its structural ordering pattern, and – *in the favorable instances* – resulting in improved device PCEs. It should be noted that the large open-circuit voltage ($V_{OC}$) values of *ca.* 0.9 V obtained in BHJ solar cells with **FBM** and **CBM** (vs. *ca.* 0.8 V for the reference PCE10:$PC_{71}BM$ solar cells, cf. details in SI) are consistent with the shallower electrochemically-estimated EAs of these two SM acceptors (*ca.* 4.1 eV) compared to that of $PC_{71}BM$ (4.1-4.3 eV); the lower $V_{OC}$ of *ca.* 0.65-0.7 V obtained with **CDTBM** is in agreement with the larger electrochemically-estimated EAs of this system (*ca.* 4.3 eV) compared to those of **FBM** and **CBM**. Interestingly, the lower $V_{OC}$ of the **CDTBM**-based BHJ devices is outweighed by the higher $J_{SC}$ and *FF* values, and overall, all SM acceptors perform comparably well.

The comparable $J_{SC}$ values achieved in optimized **FBM**-, **CBM**- and **CDTBM**-based BHJ solar cells (Fig. 2a) are consistent with the external quantum efficiency (EQE) spectra (Fig. 2b); integrated EQEs vs. $J_{SC}$: ± 0.6 mA/$cm^2$; ± 5%. Figure 2b emphasizes the significant contributions of **FBM** and **CBM** to the EQE in the range 400-600 nm (region complementary to the spectral absorption of PCE10), reaching *ca.* 70% at the SM acceptors' maximum absorp-

tion peak. In contrast, the spectral absorption of **CDTBM** reinforces that of PCE10 in the range 550-850 nm,

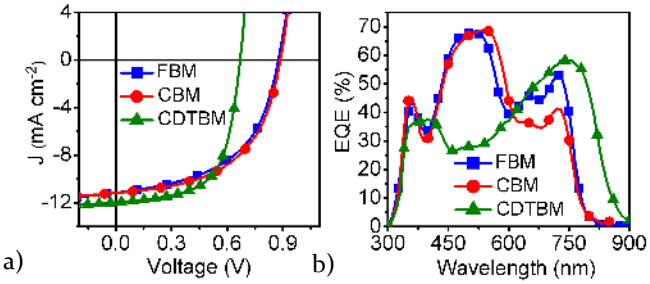


**Figure 2. (a)** Characteristic *J-V* curves of optimized BHJ solar cells fabricated from **FBM** (cast from CB, 1% CN v/v), **CBM** (cast from CB, 2% DIO v/v), and **CDTBM** (cast from CB, 0.8% CN v/v), with PCE10 as the polymer donor; AM1.5G solar illumination (100 mW/cm$^2$). **(b)** EQE spectra of the devices fabricated from the SM acceptors and PCE10 under optimized conditions. Integrated EQEs are in agreement (± 0.6 mA/cm$^2$; ± 5%) with the $J_{SC}$ values reported in Table 2.

Table 2. PV Performance of the SM Acceptors FBM, CBM and CDTBM in Inverted BHJ Devices with PCE10 as the Polymer Donor.[d]

| SM | additive %(v/v) | $J_{SC}$ [mA/cm$^2$] | $V_{OC}$ [V] | *FF* [%] | Avg. PCE[c] [%] | Max. PCE [%] |
|---|---|---|---|---|---|---|
| **FBM** | 0 | 10.8 | 0.88 | 44 | 4.2 | 4.4 |
| | 1.0[a,e] | 11.2 | 0.88 | 51 | 5.0 | 5.1 |
| **CBM** | 0 | 9.4 | 0.89 | 48 | 4.0 | 4.1 |
| | 2.0[b,e] | 10.6 | 0.88 | 53 | 5.0 | 5.3 |
| **CDTBM** | 0 | 11.7 | 0.68 | 53 | 4.2 | 4.6 |
| | 0.8[a,e] | 11.9 | 0.66 | 60 | 4.8 | 5.0 |

[a]Device with optimized PCE10:SM ratio of 4:6 (wt/wt) solution-cast from chlorobenzene (CB) with CN as processing additive. [b]Device with optimized PCE10:SM ratio of 3:7 (wt/wt) solution-cast from chlorobenzene (CB) with DIO as processing additive. [c]Average values across >20 devices (device area: 0.1 cm$^2$). [d]Additional device statistics, including standard deviations, are provided in the SI (Table. S1-S2). [e]Optimized device conditions.

contributing to the pronounced EQE response in the long-wavelength region of the visible spectrum (where high photon flux densities occur), and peaking to *ca.* 60% at the SM acceptors' absorption maximum. The onset of EQE for **CDTBM**-based BHJ solar cells is also red-shifted compared to that for **FBM** and **CBM**-based devices; observation in agreement with the absorption pattern of **CDTBM** (Fig. 1a) extending to longer wavelengths than the thin-film absorption onset of PCE10. Our transfer matrix simulations[65] shown in Figure S10 (max. theoretical $J_{SC}$ vs. active layer thickness, assuming 100% IQE; cf. details in SI) are consistent with the observation that the $J_{SC}$ values achieved in **FBM**-, **CBM**- and **CDTBM**-based devices with *ca.* 65 nm active layers fall within the same range. From these simulations, it can also be inferred that higher $J_{SC}$ values may be achievable for active layers of *ca.* 65 nm if recombination loss pathways could be suppressed (max. theoretical $J_{SC}$ at 65 nm: 17-18.5 mA/cm$^2$; estimated $J_{SC}$ losses from experimental values: 35-40%). Despite expectations of higher $J_{SC}$ values from the model, thicker active layers (*e.g.* 90 nm) cast from optimized BHJ device processing conditions did not yield higher experimental PCEs, as incremental *FF* reductions prevail in increasingly thick devices. The BHJ morphologies of "*as-cast*" and optimized **FBM**, **CBM** and **CDTBM**-based BHJ devices were examined by bright-field electron transmission microscopy (TEM; cf. details in SI). The TEM images shown in Figure 3 emphasize the development of relatively fine-scale morphologies for all nonfullerene-based active layers, consistent with the promising figures of merit discussed earlier (Table 2), including PCEs >4% both for "*as-cast*" and optimized BHJ solar cells. We note that significant differences in phase separation patterns

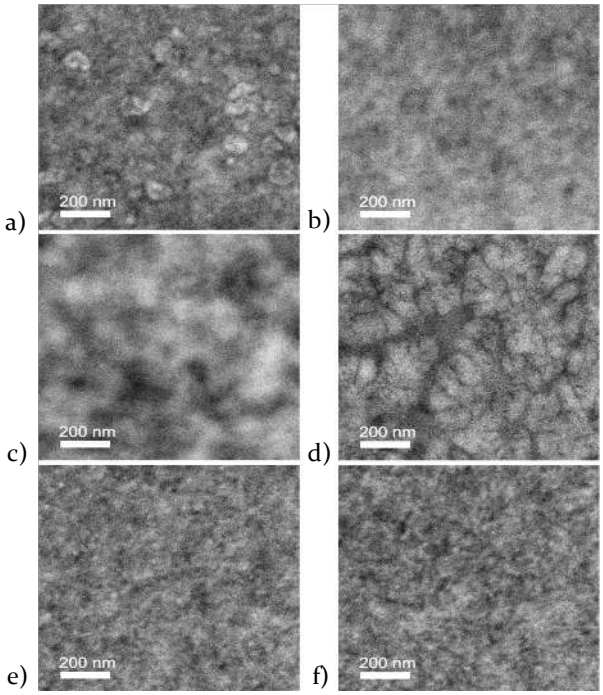


**Figure 3**. Bright-field TEM images of the BHJ thin-film morphologies with the SM acceptors **FBM**, **CBM** and **CDTBM** (cast from CB). **(a) FBM**, no additive; **(b) FBM**, 1% CN (v/v); **(c) CBM**, no additive; **(d) CBM**, 2% DIO (v/v); **(e) CDTBM**, no additive; **(f) CDTBM**, 0.8% CN (v/v).

are known to impact BHJ solar cell performance.[63-64,66] Here, the BHJ morphologies of the optimized nonfullerene-based devices appear comparably well mixed, and no clear difference in phase separation patterns can be observed at the scale of those analyses. Concurrent imaging of the topography and phase of the BHJ thin films via atomic force microscopy (AFM; cf. details in SI, Fig. S11-S13) is consistent with the expectation of homogeneous, non-aggregated active layer morphologies (root-mean-square (RMS) roughness <4 nm). These observations are

in agreement with (i) the high $J_{SC}$ values (>9 mA/cm²) achieved across the set of nonfullerene acceptors in "*as-cast*" and optimized devices (Table 2 and Fig. 2a), and (ii) the near-complete photoluminescence (PL) quenching of PCE10 in the presence of **FBM**, **CBM** and **CDTBM** as illustrated in Figures 4 and S14 (quenching efficiencies >96% in all cases, at optimized donor-acceptor ratios). Since the

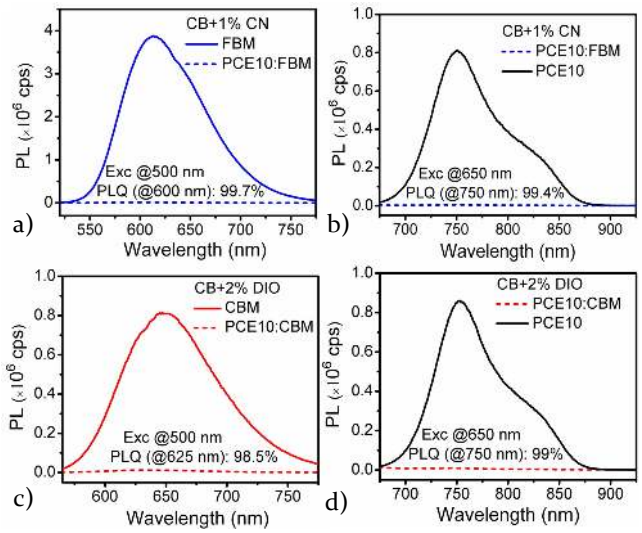


**Figure 4.** Photoluminescence (PL) quenching of PCE10 and the SM acceptor analogues **FBM** and **CBM** in neat films without additive (solid lines), and in the presence of the donor/acceptor counterpart (dashed lines) as in optimized BHJ thin films (with additive); **(a)** PCE10:**FBM**, excitation at 500 nm, **(b)** PCE10:**FBM**, excitation at 650 nm, **(c)** PCE10:**CBM**, excitation at 500 nm, **(d)** PCE10:**CBM**, excitation at 650 nm.

spectral absorptions and PL patterns of PCE10 and the SM acceptors **FBM** and **CBM** lie in regions of distinct wavelengths, the donor and acceptor components can be individually excited at different wavelengths (Fig. 4; 650 nm and 500 nm, respectively), emphasizing that both electron and hole transfers are occurring quantitatively in the BHJ active layers. Quantitative electron and hole transfers at the donor-acceptor interfaces is reflected in the EQE spectra (Fig. 2b), where both PCE10 and the SM acceptors contribute significantly to photoinduced charge generation at short-circuit. These results further indicate that morphological aspects are not limiting the diffusion of photogenerated excitons to the PCE10-rich and SM acceptor-rich domain interfaces.

In parallel, we note that our GIWAXS analyses of the optimized PCE10:SM blend films (cf. details in SI, Fig. S15) confirm the lack of SM aggregates with pronounced π-stacking correlations and long-range ordering characteristics in thin films.

While not always apparent, subtle morphological differences between BHJ thin films can sometimes translate into distinct charge transport patterns. Turning to carrier effects, we measured the hole mobilities of PCE10 and the electron mobilities of **FBM**, **CBM** and **CDTBM** in optimized BHJ thin films; values inferred from the space charge limited current (SCLC) model (cf. details in SI).

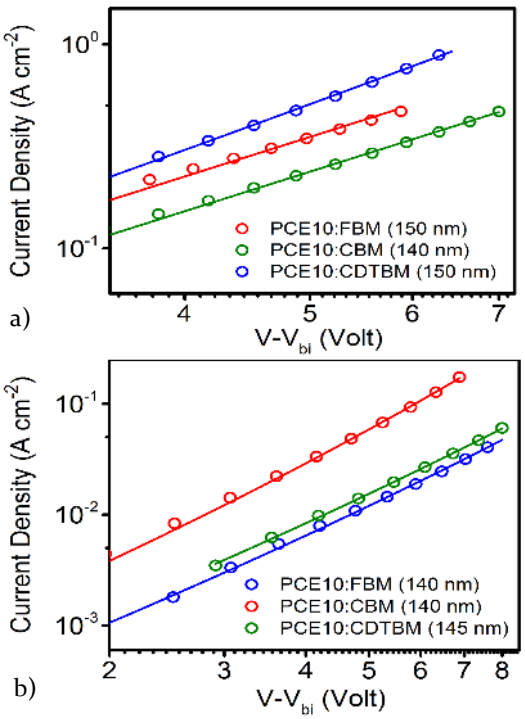


**Figure 5**. Experimental dark current densities as a function of effective electric field for (a) hole-only diodes (ITO/PEDOT/PCE10:SM/$MoO_3$/Ag); here, $V_{bi}$ = 0 (flat band pattern formed by PEDOT-$MoO_3$) and (b) electron-only diodes (ITO/a-ZnO/PFN-Ox/PCE10:SM/Ca/Al) made with optimized BHJ thin films ($V_{bi}$ = 0.4 V), with **FBM**, **CBM** and **CDTBM** as SM acceptors (film thicknesses: 140-150 nm). Data obtained for different thin thicknesses are given in SI (Fig. S16). The experimental data is fitted using the single-carrier SCLC model (solid lines; cf. details in SI).

Blends of PCE10:$PC_{71}BM$ were also examined for comparison. Hole-only diodes with the configuration ITO/PEDOT /PCE10:SM/$MoO_3$/Ag, and electron-only diodes with the configuration ITO/ZnO/PFN-Ox[67]/PCE10:SM/Ca/Al (device area: 0.1 cm²) were fabricated for these measurements and analyzed in the dark. Figure 5 shows the dark current densities of the optimized BHJ thin films in the carrier-selective diodes as a function of applied effective field (various BHJ thicknesses were examined for more accuracy in those estimations, see Fig. S16). Our analyses indicate that the zero-field hole mobilities of the PCE10:SM blends fall within the same range, with average estimated values of $1.4\times10^{-4}$, $1.0\times10^{-4}$ and $3.4\times10^{-4}$ cm² V⁻¹ s⁻¹, with **FBM**, **CBM** and **CDTBM**, respectively (see Table S3). The electron mobility curves for the PCE10:SM blends followed Poole-Frenkel-type mobility fits (electric-field activated) of the form $\mu(F) = \mu_0 \exp(\gamma F^{1/2})$, where $\mu_o$ is the zero field mobility, $\gamma$ is the Poole-Frenkel slope and $F$ is the electric field. In turn, the zero-field electron mobilities of the PCE10:SM blends were estimated to be $1.0\times10^{-6}$, $1.9\times10^{-6}$

and $1.8\times10^{-6}$ $cm^2V^{-1}s^{-1}$, with **FBM**, **CBM** and **CDTBM**, respectively (see Table S3); results indicating that the three SM acceptors transport electrons with comparable efficiency. We note, however, that the imbalance between hole and electron mobilities in the PCE10:SM blend thin films is likely to be at the origin of significant charge build-up in the optimized BHJ solar cells, limiting the *FF* and $J_{SC}$. In comparison, estimated (average) hole and electron mobilities for PCE10:$PC_{71}BM$ blends were measured to be $7.3\times10^{-4}$ $cm^2V^{-1}s^{-1}$ and $1.5\times10^{-4}$ $cm^2V^{-1}s^{-1}$, respectively; results in agreement with the higher *FF* (*ca.* 70%) and $J_{SC}$ (*ca.* 17 $mA/cm^2$) values obtained with the reference PCE10:$PC_{71}BM$ devices (cf. details in SI). In developing new SM acceptors, it will be critically important to identify systems with higher electron mobilities in BHJ thin films that can concurrently achieve more balanced carrier mobilities comparable to those of polymer donors (here, *ca.* $10^{-4}$ $cm^2 V^{-1} s^{-1}$ in BHJ thin films).

## Conclusions

In summary, we showed that 2-(benzo[*c*][1,2,5]-thiadiazol-4-ylmethylene)malononitrile (BM)-substituted SMs can be used as efficient nonfullerene acceptors in BHJ solar cells – with PCEs ≥5% achievable – independent of the π-bridge that links the two electron-deficient BM termini. Estimated EAs within range of those of common fullerene acceptors (4.0-4.3 eV) and a wider range of IPs (6.2-5.6 eV) impart the nonfullerene analogues with absorption spectra that fall within the visible range: 400-600 nm for **FBM** and **CBM**; 500-850 nm for **CDTBM**. While fullerene derivatizations and purifications can be tedious and tend to have modest effects on their optoelectronics, the ability to tune the optoelectronic properties of SM acceptors by design and the absence of isomeric byproducts produced at the synthetic stage are clear benefits. In BM-terminated SM acceptors, the modularity of the π-bridge may be amenable to higher-efficiency systems and we note that further solar cell PCE improvements may also come from the selection of alternative polymer donors. Overall, this concise study shows that BM-substituted SMs are a promising class of nonfullerene acceptors for solution-processable BHJ solar cells.

## Experimental Section

*Material Characterizations.* All compounds were characterized by NMR spectroscopy on Bruker Avance III Ultrashield Plus instruments using a 400 or 700 MHz proton frequency. High-resolution mass spectrometry (HRMS) analyses were performed on a Thermo Scientific - LTQ Velos Orbitrap MS. Synthetic methods and procedures for the syntheses of the SM acceptors are detailed in the Supporting Information (SI). Further details on UV-vis, PESA, CV, TGA, DSC, GIWAXS (neat films) and corresponding experimental conditions are developed in the SI.

*Computational Analyses.* All density functional theory (DFT) calculations were performed at the B3LYP/6-31G(d,p) level of theory with the Gaussian 09 (Revision C.01) software. Additional details and references can be found in the SI.

*Device Testing Protocols.* The BHJ solar cells were prepared on glass substrates with tin-doped indium oxide (ITO, 15 Ω $sq^{-1}$) patterned on the surface (device area: 0.1 $cm^2$). Details on substrate preparation, active layer and contact depositions are provided in the SI. *J-V* measurements were performed in the glovebox with a Keithley 2400 source meter and an Oriel Sol3A Class AAA solar simulator calibrated to 1 sun, AM1.5 G, with a KG-5 silicon reference cell certified by Newport. The external quantum efficiency (EQE) measurements were performed at zero bias by illuminating the device with monochromatic light supplied from a Xenon arc lamp in combination with a dual-grating monochromator. The number of photons incident on the sample was calculated for each wavelength by using a silicon photodiode calibrated by NIST. Additional details on various active layer deposition conditions, $J_{SC}$ modeling, BHJ thin-film UV-vis, TEM, AFM, PL instrumentation, GIWAXS (BHJ films), and carrier mobility measurements are developed in the SI.

## ASSOCIATED CONTENT

Experimental methods, characterization, and additional figures and tables. This material is available free of charge via the Internet at http://pubs.acs.org.

### Corresponding Author

*E-mail: pierre.beaujuge@kaust.edu.sa

### Author Contributions

[§]These authors contributed equally.

### Notes

The authors declare no competing financial interest.

## ACKNOWLEDGMENT

This publication is based upon work supported by the King Abdullah University of Science and Technology (KAUST) Office of Sponsored Research (OSR) under Award No. CRG_R2_13_BEAU_KAUST_1. The authors acknowledge concurrent support under Baseline Research Funding from KAUST. The authors thank KAUST ACL for technical support in the mass spectrometry analyses. W.P. and T.M. gratefully acknowledge the staff of beamline 9 at the DELTA electron storage ring in Dortmund for providing beamtime and technical support for the GIWAXS measurements. W.P. and T.M. thank Marcelina Rojek for technical support in the GIWAXS measurements.

## REFERENCES

(1) Yu, G.; Gao, J.; Hummelen, J. C.; Wudl, F.; Heeger, A. J., Polymer Photovoltaic Cells: Enhanced Efficiencies Via a Network of Internal Donor-Acceptor Heterojunctions. *Science* **1995,** *270*, 1789-1791.

(2) Zhan, X.; Facchetti, A.; Barlow, S.; Marks, T. J.; Ratner, M. A.; Wasielewski, M. R.; Marder, S. R., Rylene and Related Diimides for Organic Electronics. *Adv. Mater.* **2011,** *23*, 268-284.

(3) Brabec, C. J.; Gowrisanker, S.; Halls, J. J.; Laird, D.; Jia, S.; Williams, S. P., Polymer-Fullerene Bulk-Heterojunction Solar Cells. *Adv. Mater.* **2010,** *22*, 3839-3856.

(4) Thompson, B. C.; Frechet, J. M., Polymer-Fullerene Composite Solar Cells. *Angew. Chem. Int. Ed.* **2008,** *47*, 58-77.

(5) Huang, Y.; Kramer, E. J.; Heeger, A. J.; Bazan, G. C., Bulk Heterojunction Solar Cells: Morphology and Performance Relationships. *Chem. Rev.* **2014,** *114*, 7006-7043.
(6) Kang, H.; Uddin, M. A.; Lee, C.; Kim, K. H.; Nguyen, T. L.; Lee, W.; Li, Y.; Wang, C.; Woo, H. Y.; Kim, B. J., Determining the Role of Polymer Molecular Weight for High-Performance All-Polymer Solar Cells: Its Effect on Polymer Aggregation and Phase Separation. *J. Am. Chem. Soc.* **2015,** *137*, 2359-2365.
(7) Li, H.; Earmme, T.; Ren, G.; Saeki, A.; Yoshikawa, S.; Murari, N. M.; Subramaniyan, S.; Crane, M. J.; Seki, S.; Jenekhe, S. A., Beyond Fullerenes: Design of Nonfullerene Acceptors for Efficient Organic Photovoltaics. *J. Am. Chem. Soc.* **2014,** *136*, 14589-14597.
(8) Li, H.; Kim, F. S.; Ren, G.; Hollenbeck, E. C.; Subramaniyan, S.; Jenekhe, S. A., Tetraazabenzodifluoranthene Diimides: Building Blocks for Solution-Processable N-Type Organic Semiconductors. *Angew. Chem. Int. Ed.* **2013,** *52*, 5513-5517.
(9) Zhou, Y.; Kurosawa, T.; Ma, W.; Guo, Y.; Fang, L.; Vandewal, K.; Diao, Y.; Wang, C.; Yan, Q.; Reinspach, J.; Mei, J.; Appleton, A. L.; Koleilat, G. I.; Gao, Y.; Mannsfeld, S. C.; Salleo, A.; Ade, H.; Zhao, D.; Bao, Z., High Performance All-Polymer Solar Cell Via Polymer Side-Chain Engineering. *Adv. Mater.* **2014,** *26*, 3767-3772.
(10) Anthony, J. E., Small-Molecule, Nonfullerene Acceptors for Polymer Bulk Heterojunction Organic Photovoltaics†. *Chem. Mater.* **2011,** *23*, 583-590.
(11) Kan, B.; Li, M.; Zhang, Q.; Liu, F.; Wan, X.; Wang, Y.; Ni, W.; Long, G.; Yang, X.; Feng, H.; Zuo, Y.; Zhang, M.; Huang, F.; Cao, Y.; Russell, T. P.; Chen, Y., A Series of Simple Oligomer-Like Small Molecules Based on Oligothiophenes for Solution-Processed Solar Cells with High Efficiency. *J. Am. Chem. Soc.* **2015,** *137*, 3886-3893.
(12) Sun, K.; Xiao, Z.; Lu, S.; Zajaczkowski, W.; Pisula, W.; Hanssen, E.; White, J. M.; Williamson, R. M.; Subbiah, J.; Ouyang, J.; Holmes, A. B.; Wong, W. W.; Jones, D. J., A Molecular Nematic Liquid Crystalline Material for High-Performance Organic Photovoltaics. *Nat. Commun.* **2015,** *6*, 6013.
(13) Hu, H.; Jiang, K.; Yang, G.; Liu, J.; Li, Z.; Lin, H.; Liu, Y.; Zhao, J.; Zhang, J.; Huang, F.; Qu, Y.; Ma, W.; Yan, H., Terthiophene-Based D-A Polymer with an Asymmetric Arrangement of Alkyl Chains That Enables Efficient Polymer Solar Cells. *J. Am. Chem. Soc.* **2015,** *137*, 14149-14157.
(14) Liu, Y.; Zhao, J.; Li, Z.; Mu, C.; Ma, W.; Hu, H.; Jiang, K.; Lin, H.; Ade, H.; Yan, H., Aggregation and Morphology Control Enables Multiple Cases of High-Efficiency Polymer Solar Cells. *Nat. Commun.* **2014,** *5*, 5293.
(15) Roncali, J.; Leriche, P.; Cravino, A., From One- to Three-Dimensional Organic Semiconductors: In Search of the Organic Silicon? *Adv. Mater.* **2007,** *19*, 2045-2060.
(16) Liu, Y.; Lai, J. Y. L.; Chen, S.; Li, Y.; Jiang, K.; Zhao, J.; Li, Z.; Hu, H.; Ma, T.; Lin, H.; Liu, J.; Zhang, J.; Huang, F.; Yu, D.; Yan, H., Efficient Non-Fullerene Polymer Solar Cells Enabled by Tetrahedron-Shaped Core Based 3d-Structure Small-Molecular Electron Acceptors. *J. Mater. Chem. A* **2015,** *3*, 13632-13636.
(17) Nielsen, C. B.; Holliday, S.; Chen, H. Y.; Cryer, S. J.; McCulloch, I., Non-Fullerene Electron Acceptors for Use in Organic Solar Cells. *Acc. Chem. Res.* **2015,** *48*, 2803-2812.
(18) Lin, Y.; Zhan, X., Designing Efficient Non-Fullerene Acceptors by Tailoring Extended Fused-Rings with Electron-Deficient Groups. *Adv. Energy Mater.* **2015,** *5*, 1501063.
(19) Kanibolotsky, A. L.; Perepichka, I. F.; Skabara, P. J., Star-Shaped Pi-Conjugated Oligomers and Their Applications in Organic Electronics and Photonics. *Chem. Soc. Rev.* **2010,** *39*, 2695-2728.
(20) Lin, Y.; Li, Y.; Zhan, X., Small Molecule Semiconductors for High-Efficiency Organic Photovoltaics. *Chem. Soc. Rev.* **2012,** *41*, 4245-4272.
(21) Beaujuge, P. M.; Frechet, J. M., Molecular Design and Ordering Effects in Pi-Functional Materials for Transistor and Solar Cell Applications. *J. Am. Chem. Soc.* **2011,** *133*, 20009-20029.
(22) Coughlin, E. J.; Henson, Z. B.; Welch, G. C.; Bazan, G. C., Design and Synthesis of Molecular Donors for Solution-Processed High-Efficiency Organic Solar Cells. *Acc. Chem. Res.* **2014,** *47*, 257-270.
(23) Huang, H.; Zhou, N.; Ortiz, R. P.; Chen, Z.; Loser, S.; Zhang, S.; Guo, X.; Casado, J.; López Navarrete, J. T.; Yu, X.; Facchetti, A.; Marks, T. J., Alkoxy-Functionalized Thienyl-Vinylene Polymers for Field-Effect Transistors and All-Polymer Solar Cells. *Adv. Funct. Mater.* **2014,** *24*, 2782-2793.
(24) Li, W.; Roelofs, W. S.; Turbiez, M.; Wienk, M. M.; Janssen, R. A., Polymer Solar Cells with Diketopyrrolopyrrole Conjugated Polymers as the Electron Donor and Electron Acceptor. *Adv. Mater.* **2014,** *26*, 3304-3309.
(25) Jung, J. W.; Jo, J. W.; Chueh, C. C.; Liu, F.; Jo, W. H.; Russell, T. P.; Jen, A. K., Fluoro-Substituted N-Type Conjugated Polymers for Additive-Free All-Polymer Bulk Heterojunction Solar Cells with High Power Conversion Efficiency of 6.71%. *Adv. Mater.* **2015,** *27*, 3310-3317.
(26) McAfee, S. M.; Topple, J. M.; Hill, I. G.; Welch, G. C., Key Components to the Recent Performance Increases of Solution Processed Non-Fullerene Small Molecule Acceptors. *J. Mater. Chem. A* **2015,** *3*, 16393-16408.
(27) Sun, D.; Meng, D.; Cai, Y.; Fan, B.; Li, Y.; Jiang, W.; Huo, L.; Sun, Y.; Wang, Z., Non-Fullerene-Acceptor-Based Bulk-Heterojunction Organic Solar Cells with Efficiency over 7%. *J. Am. Chem. Soc.* **2015,** *137*, 11156-11162.
(28) Meng, D.; Sun, D.; Zhong, C.; Liu, T.; Fan, B.; Huo, L.; Li, Y.; Jiang, W.; Choi, H.; Kim, T.; Kim, J.; Sun, Y.; Wang, Z.; Heeger, A., High-Performance Solution-Processed Non-Fullerene Organic Solar Cells Based on Selenophene-Containing Perylene Bisimide Acceptor. *J. Am. Chem. Soc.* **2016,** *138*, 375-380.
(29) Zhong, Y.; Kumar, B.; Oh, S.; Trinh, M. T.; Wu, Y.; Elbert, K.; Li, P.; Zhu, X.; Xiao, S.; Ng, F.; Steigerwald, M. L.; Nuckolls, C., Helical Ribbons for Molecular Electronics. *J. Am. Chem. Soc.* **2014,** *136*, 8122-8130.
(30) Zhong, Y.; Trinh, M. T.; Chen, R.; Wang, W.; Khlyabich, P. P.; Kumar, B.; Xu, Q.; Nam, C. Y.; Sfeir, M. Y.; Black, C.; Steigerwald, M. L.; Loo, Y. L.; Xiao, S.; Ng, F.; Zhu, X. Y.; Nuckolls, C., Efficient Organic Solar Cells with Helical Perylene Diimide Electron Acceptors. *J. Am. Chem. Soc.* **2014,** *136*, 15215-15221.
(31) Zhao, J.; Li, Y.; Lin, H.; Liu, Y.; Jiang, K.; Mu, C.; Ma, T.; Lin Lai, J. Y.; Hu, H.; Yu, D.; Yan, H., High-Efficiency Non-Fullerene Organic Solar Cells Enabled by a Difluorobenzothiadiazole-Based Donor Polymer Combined with a Properly Matched Small Molecule Acceptor. *Energy Environ. Sci.* **2015,** *8*, 520-525.
(32) Cai, Y.; Huo, L.; Sun, X.; Wei, D.; Tang, M.; Sun, Y., High Performance Organic Solar Cells Based on a Twisted Bay-Substituted Tetraphenyl Functionalized Perylenediimide Electron Acceptor. *Adv. Energy Mater.* **2015**, *5*, 1500032.
(33) Ren, Y.; Hailey, A. K.; Hiszpanski, A. M.; Loo, Y.-L., Isoindigo-Containing Molecular Semiconductors: Effect of Backbone Extension on Molecular Organization and Organic Solar Cell Performance. *Chem. Mater.* **2014,** *26*, 6570-6577.
(34) Liu, Y.; Zhang, L.; Lee, H.; Wang, H. W.; Santala, A.; Liu, F.; Diao, Y.; Briseno, A. L.; Russell, T. P., NDI-Based Small Molecule as Promising Nonfullerene Acceptor for Solution-Processed Organic Photovoltaics. *Adv. Energy Mater.* **2015,** *5*, 1500195.

(35) Ahmed, E.; Ren, G.; Kim, F. S.; Hollenbeck, E. C.; Jenekhe, S. A., Design of New Electron Acceptor Materials for Organic Photovoltaics: Synthesis, Electron Transport, Photophysics, and Photovoltaic Properties of Oligothiophene-Functionalized Naphthalene Diimides. *Chem. Mater.* **2011,** *23*, 4563-4577.
(36) Earmme, T.; Hwang, Y. J.; Murari, N. M.; Subramaniyan, S.; Jenekhe, S. A., All-Polymer Solar Cells with 3.3% Efficiency Based on Naphthalene Diimide-Selenophene Copolymer Acceptor. *J. Am. Chem. Soc.* **2013,** *135*, 14960-14963.
(37) Wu, X.-F.; Fu, W.-F.; Xu, Z.; Shi, M.; Liu, F.; Chen, H.-Z.; Wan, J.-H.; Russell, T. P., Spiro Linkage as an Alternative Strategy for Promising Nonfullerene Acceptors in Organic Solar Cells. *Adv. Funct. Mater.* **2015,** *25*, 5954-5966.
(38) Jung, J. W.; Jo, W. H., Low-Bandgap Small Molecules as Non-Fullerene Electron Acceptors Composed of Benzothiadiazole and Diketopyrrolopyrrole for All Organic Solar Cells. *Chem. Mater.* **2015,** *27*, 6038-6043.
(39) Lin, Y.; Cheng, P.; Li, Y.; Zhan, X., A 3d Star-Shaped Non-Fullerene Acceptor for Solution-Processed Organic Solar Cells with a High Open-Circuit Voltage of 1.18 V. *Chem. Commun.* **2012,** *48*, 4773-4775.
(40) Douglas, J. D.; Chen, M. S.; Niskala, J. R.; Lee, O. P.; Yiu, A. T.; Young, E. P.; Frechet, J. M., Solution-Processed, Molecular Photovoltaics That Exploit Hole Transfer from Non-Fullerene, N-Type Materials. *Adv. Mater.* **2014,** *26*, 4313-4319.
(41) Bloking, J. T.; Giovenzana, T.; Higgs, A. T.; Ponec, A. J.; Hoke, E. T.; Vandewal, K.; Ko, S.; Bao, Z.; Sellinger, A.; McGehee, M. D., Comparing the Device Physics and Morphology of Polymer Solar Cells Employing Fullerenes and Non-Fullerene Acceptors. *Adv. Energy Mater.* **2014,** *4*, 1301426.
(42) Bloking, J. T.; Han, X.; Higgs, A. T.; Kastrop, J. P.; Pandey, L.; Norton, J. E.; Risko, C.; Chen, C. E.; Brédas, J.-L.; McGehee, M. D.; Sellinger, A., Solution-Processed Organic Solar Cells with Power Conversion Efficiencies of 2.5% Using Benzothiadiazole/Imide-Based Acceptors. *Chem. Mater.* **2011,** *23*, 5484-5490.
(43) Kim, Y.; Song, C. E.; Moon, S. J.; Lim, E., Rhodanine Dye-Based Small Molecule Acceptors for Organic Photovoltaic Cells. *Chem. Commun.* **2014,** *50*, 8235-8238.
(44) Wu, Y.; Bai, H.; Wang, Z.; Cheng, P.; Zhu, S.; Wang, Y.; Ma, W.; Zhan, X., A Planar Electron Acceptor for Efficient Polymer Solar Cells. *Energy Environ. Sci.* **2015,** *8*, 3215-3221.
(45) Holliday, S.; Ashraf, R. S.; Nielsen, C. B.; Kirkus, M.; Rohr, J. A.; Tan, C. H.; Collado-Fregoso, E.; Knall, A. C.; Durrant, J. R.; Nelson, J.; McCulloch, I., A Rhodanine Flanked Nonfullerene Acceptor for Solution-Processed Organic Photovoltaics. *J. Am. Chem. Soc.* **2015,** *137*, 898-904.
(46) Kamm, V.; Battagliarin, G.; Howard, I. A.; Pisula, W.; Mavrinskiy, A.; Li, C.; Müllen, K.; Laquai, F., Polythiophene:Perylene Diimide Solar Cells - the Impact of Alkyl-Substitution on the Photovoltaic Performance. *Adv. Energy Mater.* **2011,** *1*, 297-302.
(47) Yan, Q.; Zhou, Y.; Zheng, Y.-Q.; Pei, J.; Zhao, D., Towards Rational Design of Organic Electron Acceptors for Photovoltaics: A Study Based on Perylenediimide Derivatives. *Chem. Sci.* **2013,** *4*, 4389-4394.
(48) Kwon, O. K.; Park, J. H.; Kim, D. W.; Park, S. K.; Park, S. Y., An All-Small-Molecule Organic Solar Cell with High Efficiency Nonfullerene Acceptor. *Adv. Mater.* **2015,** *27*, 1951-1956.
(49) Lin, H.; Chen, S.; Li, Z.; Lai, J. Y.; Yang, G.; McAfee, T.; Jiang, K.; Li, Y.; Liu, Y.; Hu, H.; Zhao, J.; Ma, W.; Ade, H.; Yan, H., High-Performance Non-Fullerene Polymer Solar Cells Based on a Pair of Donor-Acceptor Materials with Complementary Absorption Properties. *Adv. Mater.* **2015**, *27*, 7299-7304.
(50) Lin, Y.; Wang, J.; Zhang, Z. G.; Bai, H.; Li, Y.; Zhu, D.; Zhan, X., An Electron Acceptor Challenging Fullerenes for Efficient Polymer Solar Cells. *Adv. Mater.* **2015,** *27*, 1170-1174.
(51) Winzenberg, K. N.; Kemppinen, P.; Scholes, F. H.; Collis, G. E.; Shu, Y.; Singh, T. B.; Bilic, A.; Forsyth, C. M.; Watkins, S. E., Indan-1,3-Dione Electron-Acceptor Small Molecules for Solution-Processable Solar Cells: A Structure-Property Correlation. *Chem. Commun.* **2013,** *49*, 6307-6309.
(52) Lin, Y.; Zhang, Z.-G.; Bai, H.; Wang, J.; Yao, Y.; Li, Y.; Zhu, D.; Zhan, X., High-Performance Fullerene-Free Polymer Solar Cells with 6.31% Efficiency. *Energy Environ. Sci.* **2015,** *8*, 610-616.
(53) Zhong, Y.; Trinh, M. T.; Chen, R.; Purdum, G. E.; Khlyabich, P. P.; Sezen, M.; Oh, S.; Zhu, H.; Fowler, B.; Zhang, B.; Wang, W.; Nam, C. Y.; Sfeir, M. Y.; Black, C. T.; Steigerwald, M. L.; Loo, Y. L.; Ng, F.; Zhu, X. Y.; Nuckolls, C., Molecular Helices as Electron Acceptors in High-Performance Bulk Heterojunction Solar Cells. *Nat. Commun.* **2015,** *6*, 8242.
(54) Bai, H.; Wang, Y.; Cheng, P.; Wang, J.; Wu, Y.; Hou, J.; Zhan, X., An Electron Acceptor Based on Indacenodithiophene and 1,1-Dicyanomethylene-3-Indanone for Fullerene-Free Organic Solar Cells. *J. Mater. Chem. A* **2015,** *3*, 1910-1914.
(55) Lin, L.-Y.; Chen, Y.-H.; Huang, Z.-Y.; Lin, H.-W.; Chou, S.-H.; Lin, F.; Chen, C.-W.; Liu, Y.-H.; Wong, K.-T., A Low Energy Gap Organic Dye for High-Performance Small Molecule Organic Solar Cells. *J. Am. Chem. Soc.* **2011,** *133*, 15822-15825.
(56) Lin, L. Y.; Lu, C. W.; Huang, W. C.; Chen, Y. H.; Lin, H. W.; Wong, K. T., New A-A-D-A-A-Type Electron Donors for Small Molecule Organic Solar Cells. *Org. Lett.* **2011,** *13*, 4962-4965.
(57) Fang, Y.; Pandey, A. K.; Nardes, A. M.; Kopidakis, N.; Burn, P. L.; Meredith, P., A Narrow Optical Gap Small Molecule Acceptor for Organic Solar Cells. *Adv. Energy Mater.* **2013,** *3*, 54-59.
(58) Wolfer, P.; Schwenn, P. E.; Pandey, A. K.; Fang, Y.; Stingelin, N.; Burn, P. L.; Meredith, P., Identifying the Optimum Composition in Organic Solar Cells Comprising Non-Fullerene Electron Acceptors. *J. Mater. Chem. A* **2013,** *1*, 5989-5995.
(59) Che, X.; Xiao, X.; Zimmerman, J. D.; Fan, D.; Forrest, S. R., High-Efficiency, Vacuum-Deposited, Small-Molecule Organic Tandem and Triple-Junction Photovoltaic Cells. *Adv. Energy Mater.* **2014,** *4*, 1400568.
(60) Bai, H.; Wu, Y.; Wang, Y.; Wu, Y.; Li, R.; Cheng, P.; Zhang, M.; Wang, J.; Ma, W.; Zhan, X., Nonfullerene Acceptors Based on Extended Fused Rings Flanked with Benzothiadiazolylmethylenemalononitrile for Polymer Solar Cells. *J. Mater. Chem. A* **2015,** *3*, 20758-20766.
(61) Jagadamma, L. K.; Abdelsamie, M.; El Labban, A.; Aresu, E.; Ngongang Ndjawa, G. O.; Anjum, D. H.; Cha, D.; Beaujuge, P. M.; Amassian, A., Efficient Inverted Bulk-Heterojunction Solar Cells from Low-Temperature Processing of Amorphous Zno Buffer Layers. *J. Mater. Chem. A* **2014,** *2*, 13321-13331.
(62) Zhang, S.; Ye, L.; Zhao, W.; Liu, D.; Yao, H.; Hou, J., Side Chain Selection for Designing Highly Efficient Photovoltaic Polymers with 2d-Conjugated Structure. *Macromolecules* **2014,** *47*, 4653-4659.
(63) Cabanetos, C.; El Labban, A.; Bartelt, J. A.; Douglas, J. D.; Mateker, W. R.; Frechet, J. M.; McGehee, M. D.; Beaujuge, P. M., Linear Side Chains in Benzo[1,2-*b*:4,5-*b*']Dithiophene-Thieno[3,4-*c*]Pyrrole-4,6-Dione Polymers Direct Self-Assembly and Solar Cell Performance. *J. Am. Chem. Soc.* **2013,** *135*, 4656-4659.
(64) Warnan, J.; El Labban, A.; Cabanetos, C.; Hoke, E. T.; Shukla, P. K.; Risko, C.; Brédas, J.-L.; McGehee, M. D.; Beaujuge, P. M., Ring Substituents Mediate the Morphology of Pbdttpd-Pcbm Bulk-Heterojunction Solar Cells. *Chem. Mater.* **2014,** *26*, 2299-2306.

(65) Pettersson, L.; Roman, L.; Inganäs, O., Modeling Photocurrent Action Spectra of Photovoltaic Devices based on Organic Thin Films. *J. Appl. Phys.* **1999**, *86*, 487-496.
(66) Warnan, J.; Cabanetos, C.; Bude, R.; El Labban, A.; Li, L.; Beaujuge, P. M., Electron-Deficientn-Alkyloyl Derivatives of Thieno[3,4-*c*]Pyrrole-4,6-Dione Yield Efficient Polymer Solar Cells with Open-Circuit Voltages > 1 V. *Chem. Mater.* **2014,** *26*, 2829-2835.
(67) Liu, S.; Zhang, K.; Lu, J.; Zhang, J.; Yip, H.-L.; Huang, F.; Cao, Y., High-efficiency Polymer Solar Cells via the Incorporation of an Amino-Functionalized Conjugated Metallopolymer as a Cathode Interlayer. *J. Am. Chem. Soc.* **2013**, *135*, 15326-15329.

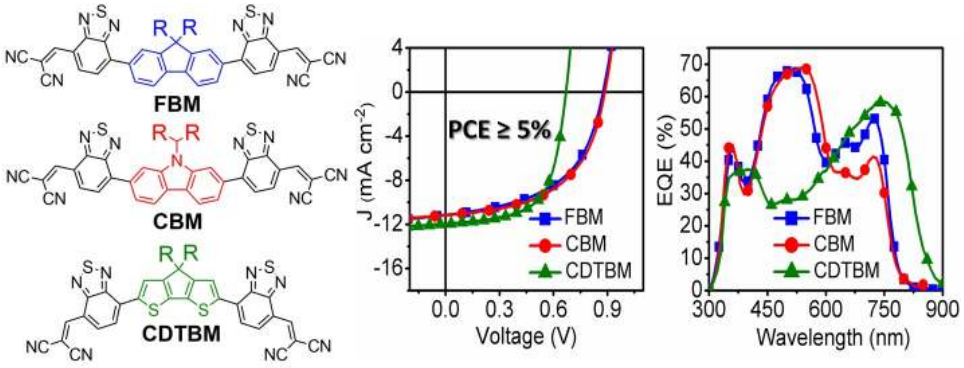
FBM
CBM
CDTBM
PCE ≥ 5%
J (mA cm-2)
Voltage (V)
EQE (%)
Wavelength (nm)
FBM
CBM
CDTBM